

WiFi-based Multi-task Sensing

Xie Zhang¹, Chengpei Tang¹, Yasong An¹, and Kang Yin¹

¹ Sun Yat-sen University, Guangzhou 510006, China

Abstract. WiFi-based sensing has aroused immense attention over recent years. The rationale is that the signal fluctuations caused by humans carry the information of human behavior which can be extracted from the channel state information of WiFi. Still, the prior studies mainly focus on single-task sensing (STS), e.g., gesture recognition, indoor localization, user identification. Since the fluctuations caused by gestures are highly coupling with body features and the user's location, we propose a WiFi-based multi-task sensing model (Wimuse) to perform gesture recognition, indoor localization, and user identification tasks simultaneously. However, these tasks have different difficulty levels (i.e., imbalance issue) and need task-specific information (i.e., discrepancy issue). To address these issues, the knowledge distillation technique and task-specific residual adaptor are adopted in Wimuse. We first train the STS model for each task. Then, for solving the imbalance issue, the extracted common feature in Wimuse is encouraged to get close to the counterpart features of the STS models. Further, for each task, a task-specific residual adaptor is applied to extract the task-specific compensation feature which is fused with the common feature to address the discrepancy issue. We conduct comprehensive experiments on three public datasets and evaluation suggests that Wimuse achieves state-of-the-art performance with the average accuracy of 85.20%, 98.39%, and 98.725% on the joint task of gesture recognition, indoor localization, and user identification, respectively.

Keywords: Channel State Information, Gesture recognition, Human identification, Knowledge Distillation, Localization, Multi-task Learning, WiFi-based sensing.

1 Introduction

WiFi-based sensing has drawn considerable interest over recent years due to its pervasive availability, non-intrusiveness, and low-cost deployment. Numerous studies [1]–[3] have shown that WiFi-based human sensing can be regarded as a promising candidate to promote human-computer interaction in the Internet of Things (IoT) era. The basic principle of WiFi-based sensing is that some of the signals are absorbed, reflected, or scattered by humans on the propagation, leading to the signal fluctuations which carry the information of human behavior. Further, the signal fluctuations are described by the channel state information (CSI) of WiFi, which can be captured from commercial WiFi devices [4], [5].

2.3 Knowledge Distillation

Knowledge distillation (KD), proposed by Hinton et al. [15], is dedicated to transforming the learned knowledge in an ensemble of models into a single model and is adopted in model compression [32], transfer learning [33], domain adaptation [34], and multimodal learning [35], etc.

In addition to success in single-task learning, knowledge distillation has also been proved to be efficient in multi-task learning. Dan Xu et al. [36] proposed a novel multi-task guided prediction-and-distillation network to perform the joint tasks for depth estimation and scene parsing. Sahil Chelaramani et al. [37] proposed the use of multi-task learning and knowledge distillation to improve fine-grained recognition of eye diseases using a small labeled dataset of fundus images.

In this work, we adopt the knowledge distillation technique to address the task-imbalance issue, which is inspired by the knowledge distillation-based method [13]. In addition, to sufficiently exploit the trained STS model, we add a new loss in Wiumuse to encourage the predictive logits for each task to get closer to that produced by the corresponding trained STS model. The experimental results conduct that this trick can promote the performance of Wiumuse.

Fig. 1. The framework of Wiumuse (an example in the two-task condition, i.e. user identification and gesture recognition). We first train the task-specific STS model for each task (i.e. (a) and (c)). Then, freezing the learned parameters of the STS models. In the training phase of Wiumuse, we optimize the parameters by minimizing the losses.

3 Methodology

In this section, we present the framework of Wimuse as shown in Fig. 1. Concretely, we first introduce the input and four basic modules (i.e., shallow encoder, deep encoder, task-specific residual adaptor, and classifier). Then, we will discuss the STS model and the naïve MTS model. Finally, Wimuse is proposed.

3.1 Overview

As illustrated in Fig.1, we adopt the CSI sample as input to implement the sensing tasks. Specifically, CSI reflects multipath fluctuations of WiFi signal on all subcarriers. For each subcarrier, we can model the channel impulse response as:

$$h(t) = \sum_{i=0}^{I-1} a_i \delta(t - \tau_i) e^{-j2\pi f_i t} \quad (1)$$

where I denotes the number of signal paths. a_i , $2\pi f_i$, and τ_i are the attenuation factor, phase shift, and time delay of the signal on the i -th path, respectively. In addition, f_i represents the frequency of subcarrier, $\delta(t)$ is the Dirac delta function.

Further, the orthogonal frequency division multiplexing receiver can sample the CIR in all subcarriers to construct a complex matrix, i.e., a CSI matrix. Hence that, CSI can be denoted as:

$$H = \|H\| e^{j\angle H} \quad (2)$$

where H denotes the CSI measurement on all subcarriers. $\|H\|$ and $\angle H$ represent the amplitude and phase, respectively.

In this work, we adopt $\|H\| \in R^{L \times S \times T}$ as input, where L is the number of links, namely, $L = RX \times TX$, RX and TX is the number of antennas of the receiver and the transmitter. S denotes the number of subcarriers. P represents the length of sampling, which is determined by the sampling rate r of the CSI capture tool and the gesture execution time t (i.e., $P = r \times t$). hence that, the input $\|H\| \in R^{L \times S \times P}$ can be regarded as the reflection of signal fluctuations on three dimensions, i.e., spatial, frequency, and time.

In addition, we provide four basic modules to construct the STS model, the naïve MTS model, and Wimuse. Note that the implementation details of these modules are presented in Section IV, while a brief introduction is as follows.

- i. **shallow encoder (SE)**: For extracting the features on links of input $\|H\| \in R^{L \times S \times P}$, the shallow encoder, denoted as $\varphi(\cdot)$, contains a grouping convolutional layer and a max-pooling layer, where the number of groups equals the number of links L .
- ii. **deep encoder (DE)**: By using the low-level features extracted by the Shallow Encoder as input, a deeper convolutional subnetwork $\phi(\cdot)$ is adopted to fusion the features of different links and extract high-level features. In addition, this module is constructed based on the structure of ResNet [38].
- iii. **task-specific residual adaptor (RA)**: To deal with the task discrepancy issue, a Task-specific residual adaptor $f(\cdot)$, which contains only one convolutional layer, is adopted in the Wimuse to gain the task-specific compensation feature from the

low-level features.

- iv. **classifier:** For each classification task, a classifier $C(\cdot)$, which contains a convolutional layer and a fully connected layer, is adopted to output the logits. Then, by using the softmax function on the predictive logits, the probability over categories is produced.

Note that, all the convolutional layers in the above modules adopt one-dimensional convolution along the time dimension of CSI. We using superscripts st , mt , and wi to denote the modules in the STS model, the naïve MTS model, and the Wimuse model, respectively. In addition, the subscript of the above modules' symbols represents the task, i.e., UI denotes user identification, GR is the gesture recognition, and IL presents indoor localization. For example, $C_{UI}^{st}(\cdot)$ presents the Classifier module of an STS model at the user identification task.

3.2 Single-task Sensing Model

Consider that we have a dataset D that contains N training CSI samples H_n and their labels $y_n \in \{1, 2, \dots, M\}$, for $n \in \{1, 2, \dots, N\}$, where M is the number of categories. In this case, the STS model is composed of three parts: **i**) a shallow encoder $\varphi^{st}(\cdot; \theta^{st})$, where θ^{st} are the learned parameters. Given a CSI sample H_n as input, the output of $\varphi^{st}(\cdot; \theta^{st})$ is the low-level features on all links, i.e. $F_n^{st,low} = \varphi^{st}(H_n; \theta^{st})$. **ii**) a deep encoder $\phi^{st}(\cdot; \delta^{st})$ is adopted to fusion the low-level features across links and map to high-level features $F^{st,high}$, where δ^{st} denotes the learned parameters. Hence, the output of the Deep Encoder is $F_n^{st,high} = \phi^{st}(\cdot; \delta^{st}) \circ \varphi^{st}(H_n; \theta^{st})$. **iii**) To output the predictive probability distribution over categories, a classifier $C(\cdot; \xi^{st})$ is used to output the predictive logits $\mathbf{Z}^{st} \in R^M$, where ξ^{st} presents the learned parameters. Particularly, the predictive logits of H_n is $\mathbf{Z}_n^{st} = C(\cdot; \xi^{st}) \circ \phi^{st}(\cdot; \delta^{st}) \circ \varphi^{st}(H_n; \theta^{st})$. Then, the predictive probability distribution p_n of H_n over categories is produced by using the softmax function as follows:

$$p_n(\widehat{y}_n = m | H_n) = \sigma(\mathbf{Z}_n^{st})_m \quad (3)$$

where \widehat{y}_n is the predicted label of H_n and $m \in \{1, 2, \dots, M\}$. $\sigma(\cdot)_m$ is the softmax function, defined as:

$$\sigma(\mathbf{Z})_m = \frac{e^{Z_m}}{\sum_{k=1}^M e^{Z_k}}, \text{ for } \mathbf{Z} \in \mathbf{R}^M, m \in \{1, 2, \dots, M\} \quad (4)$$

To optimize the parameters of the STS model, a loss function $l^{st}(\cdot, \cdot)$ based on cross-entropy is adopted. The loss for H_n is as follows:

$$l^{st}(p_n, y_n) = - \sum_{m=1}^M (1|y_n = m) \log(p_n(\widehat{y}_n = m | H_n)) \quad (5)$$

where $(1|y_n = m)$ means if $y_n = m$ is true, $(1|y_n = m)$ equals 1, otherwise, 0.

The goal is to minimize the sum of losses overall training samples.

$$(\theta_{opt}^{st}, \delta_{opt}^{st}, \xi_{opt}^{st}) = \arg \min_{\theta^{st}, \delta^{st}, \xi^{st}} \sum_{n=1}^N l^{st}(p_n, y_n) \quad (6)$$

3.3 Naïve Multi-task Sensing Model

The naïve MTS model is based on the classic multi-task learning model proposed in [26]. Specifically, the naïve MTS model has only one difference from the STS model. Consider that we are given a dataset D containing N training CSI samples H_n and their labels \mathbf{y}_n where $n \in \{1, 2, \dots, N\}$. Note that, there are T tasks to performance, i.e. $\mathbf{y}_n \in R^T$. The element $y_{t,n} \in \{1, 2, \dots, M_t\}$ is the label of H_n on the t -th task, where M_t is the number of categories on the t -th task.

The naïve MTS model has the same encoder structure as the above STS model. Then the high-level features $F_n^{mt,high}$ of H_n is $\phi^{mt}(\cdot; \delta^{mt}) \circ \varphi^{mt}(H_n; \theta^{mt})$. Compared with the STS model, there are T classifiers in the naïve MTS model, e.g. $C_t^{mt}(\cdot; \xi^{mt})$ is the classifier of the t -th task. Further, the predictive logits of H_n on the t -th task is $\mathbf{Z}_{t,n}^{mt} = C_t^{mt}(\cdot; \xi^{mt}) \circ \phi^{mt}(\cdot; \delta^{mt}) \circ \varphi^{mt}(H_n; \theta^{mt}) \in R^{M_t}$. Finally, the predictive probability distribution of H_n over category on the t -th task is:

$$p_{t,n}(\widehat{y}_{t,n} = m_t | H_n) = \sigma(\mathbf{Z}_{t,n}^{mt})_{m_t}, \text{ for } m_t \in \{1, 2, \dots, M_t\} \quad (7)$$

where $\widehat{y}_{t,n}$ is the predicted label of H_n on the t -th task, $m_t \in \{1, 2, \dots, M_t\}$. $\sigma(\cdot)_{m_t}$ is the softmax function as (4).

The loss function for the t -th task $l_t^{mt}(\cdot, \cdot)$ in naïve MTS model is the same as that in STS model, i.e. $l_t^{mt}(p_{t,n}, y_{t,n}) = l^{st}(p_{t,n}, y_{t,n})$. Then the linear combination of all the task-specific loss constructs the final loss of the naïve MTS model, namely,

$$l^{mt}(\mathbf{p}_n, \mathbf{y}_n) = \sum_{t=1}^T \omega_t l_t^{mt}(p_{t,n}, y_{t,n}) \quad (8)$$

where ω_t is a hyperparameter for the t -th task, $\mathbf{p}_n = \{p_{1,n}, p_{2,n}, \dots, p_{T,n}\}$ is the set of predictive probability distributions of the sample H_n of all tasks.

Finally, the naïve MTS model can be learned by optimizing the following loss:

$$(\theta^{mt}, \delta^{mt}, \xi_1^{mt}, \xi_2^{mt}, \dots, \xi_T^{mt})_{opt} = \arg \min_{\theta^{mt}, \delta^{mt}, \xi_1^{mt}, \xi_2^{mt}, \dots, \xi_T^{mt}} \sum_{n=1}^N \sum_{t=1}^T \omega_t l_t^{mt}(p_{t,n}, y_{t,n}) \quad (9)$$

3.4 Wimuse Model

The Wimuse model is based on the naïve MTS model while introducing the knowledge distillation method and task-specific residual adaptor to address the task imbalance and discrepancy issues.

Given the same dataset D as the above MTS model. In this case, the Wimuse model is composed as following parts:

i) We first adopt a shallow encoder, denoted as $\varphi^{wi}(\cdot; \theta^{wi})$, to extract the low-level features on all links, θ^{wi} is the learned parameters. For example, the low-level features of the sample H_n is $F_n^{wi,low} = \varphi^{wi}(H_n; \theta^{wi})$.

ii) To address the task discrepancy issue, we adopt a task-specific residual adaptor $f(\cdot; \sigma^{wi})$ for each task to extract the task-specific compensation feature, denoted as $F^{wi,comp}$. For example, the task-specific compensation feature of H_n at the t -th task is $F_{t,n}^{wi,comp} = f_t(\cdot; \sigma_t^{wi}) \circ \varphi^{wi}(H_n; \theta^{wi})$.

iii) The common feature $F_n^{wi,comm}$ of sample H_n for all tasks are extracted by a deep encoder $\phi^{wi}(\cdot; \delta^{wi})$ using $F_n^{wi,low}$ as input, i.e. $F_n^{wi,comm} = \phi^{wi}(F_n^{wi,low}; \delta^{wi})$.

iv) Similar to the MTS model, Wimuse also have T classifiers, e.g. for the t – th task, the classifier is $C_t^{wi}(\cdot; \xi_t^{wi})$. Note that, the input for each classifier is the composition of the corresponding task-specific compensation feature and the common features. For example, the input for $C_t^{wi}(\cdot; \xi_t^{wi})$ of the sample H_n is $F_{t,n}^{wi,comp} \oplus F_n^{wi,comm}$, where \oplus presents the concatenate operation. In addition, the output of $C_t^{wi}(\cdot; \xi_t^{wi})$, for the sample H_n , is the predictive logits of the t-th task, i.e.

$$\mathbf{Z}_{t,n}^{wi} = C_t^{wi}(F_{t,n}^{wi,comp} \oplus F_n^{wi,comm}; \xi_t^{wi}) \quad (10)$$

For the task imbalance issue, a knowledge-distillation-based method [13] is adopted in Wimuse. Concretely, for each task, we first train an STS model, e.g. for the t-th task, we train an STS model $M_t^{st}(\cdot; \theta^{st}, \delta^{st}, \xi^{st})$. Then we freeze the learned parameters of this model. Further, with an input H_n , M_t^{st} can provide the high-level features $F_{t,n}^{st,high}$ and the logits $\mathbf{Z}_{t,n}^{st}$ for the t-th task. Then, at the training phase of Wimuse, we construct a loss function $l_t^{kd1}(\cdot, \cdot)$ to encourage the common feature $F_n^{wi,comm}$, extracted by Wimuse, to get close to all of the high-level features produced by the trained STL models after a linear transform under the Euclidean distance. For example, for the t-th task on the sample H_n , the loss $l_{t,n}^{kd1}$ is as follows:

$$l_{t,n}^{kd1} = \left\| \frac{LT_t(F_n^{wi,comm})}{\|LT_t(F_n^{wi,comm})\|_2} - \frac{F_{t,n}^{st,high}}{\|F_{t,n}^{st,high}\|_2} \right\|_2 \quad (11)$$

where $LT_t(\cdot)$ is the linear transform for the t-th task, which is implemented as a $1 \times 1 \times C \times C$ convolution, where C is the depth (number of channels) of $F_n^{wi,comm}$.

Furthermore, to sufficiently exploit the trained STS models, we also encourage the predictive logits $\mathbf{Z}_{t,n}^{wi}$ to be similar with the logits $\mathbf{Z}_{t,n}^{st}$ for sample H_n on the t-th task, which leads to another loss:

$$l_{t,n}^{kd2} = - \sum_{m_t=1}^{M_t} (P_{1,m_t} \cdot \log(P_{2,m_t})) \quad (12)$$

Where P_{1,m_t} and P_{2,m_t} is the predictive probability distribution based on $\mathbf{Z}_{t,n}^{wi}$ and $\mathbf{Z}_{t,n}^{st}$, calculated as follows:

$$P_{1,m_t} = \sigma \left(\frac{\mathbf{Z}_{t,n}^{wi}}{\boldsymbol{\tau}} \right)_{m_t} \quad (13)$$

$$P_{2,m_t} = \sigma \left(\frac{\mathbf{Z}_{t,n}^{st}}{\boldsymbol{\tau}} \right)_{m_t} \quad (14)$$

Where $\sigma(\cdot)_{m_t}$ is the softmax function as (4). And $\boldsymbol{\tau}$ is a hyperparameter to adjust the intensity of distillation [15].

The final output of Wimuse for input sample H_n is a set of the probability distribution $\mathbf{p}_n =$

$\{p_{1,n}, p_{2,n}, \dots, p_{T,n}\}$ of all T tasks. The element is defined as follows:

$$p_{t,n}(\widehat{y}_{t,n} = m_t | H_n) = \sigma(\mathbf{Z}_{t,n}^{wi})_{m_t} \quad (15)$$

where $\widehat{y}_{t,n}$ is the predicted label of H_n on the t-th task, and $m_t \in \{1, 2, \dots, M_t\}$. $\sigma(\cdot)_{m_t}$ is the softmax function as (4).

The loss function for the final prediction is as follows,

$$l^{wi}(\mathbf{p}_n, \mathbf{y}_n) = \sum_{t=1}^T \omega_t l_t^{wi}(p_{t,n}, y_{t,n}) \quad (16)$$

where ω_t is a hyperparameter for the t-th task and $l_t^{wi}(\cdot, \cdot)$ is identical with $l^{st}(\cdot, \cdot)$ (refer to (5)).

The parameters of Wimuse can be learned by minimizing the following loss:

$$l(D) = \sum_{n=1}^N \sum_{t=1}^T (\omega_t l_t^{wi}(p_{t,n}, y_{t,n}) + \lambda l_{t,n}^{kd_1} + l_{t,n}^{kd_2}) \quad (17)$$

where D is the training set and λ is the weight of the loss $l_t^{kd_1}$.

Algorithm 1: Episode-based training for Wimuse

$\boldsymbol{\varphi}_t^{st}(\cdot)$: the pre-trained shallow encoder of single task model (STM) for t-th task.
 $\boldsymbol{\Phi}_t^{st}(\cdot)$: the pre-trained deep encoder of STM for t-th task.
 $\mathbf{C}_t^{st}(\cdot)$: the pre-trained classifier of STM for t-th task.
 $\boldsymbol{\varphi}^{wi}(\cdot)$: the shallow encoder of Wimuse.
 $\boldsymbol{\Phi}^{wi}(\cdot)$: the deep encoder of Wimuse.
 $\mathbf{C}_t^{wi}(\cdot)$: the classifier of the t-th task in Wimuse.
 $f_t(\cdot)$: the task-specific residual adaptor of Wimuse for the t-th task.

Input: Training set $P = \{(x_i, y_{t,i})\}_{i=1}^N$, where $y_{t,i} \in \{1, 2, \dots, M_t\}$ is the label of sample x_i on the t-th task, and where M_t is the number of categories on the t-th task.

Output: The loss J of a randomly generated episode.

Beginning:

Give a sample $(x_i, y_{t,i})$ from P randomly.

$$\mathbf{F}^{wi,comm} = \boldsymbol{\Phi}^{wi}(\cdot) \circ \boldsymbol{\varphi}^{wi}(x_i).$$

// calculate the common feature in Wimuse

$$\mathbf{F}_{t,i}^{wi,comp} = f_t(\cdot) \circ \boldsymbol{\varphi}^{wi}(x_i)$$

// calculate the compensation feature of the t-th task in Wimuse

for t in {1, 2, ... T} do

$$\mathbf{Z}_t^{wi} = \mathbf{C}_t^{wi}(\mathbf{F}_{t,n}^{wi,comp} \oplus \mathbf{F}_n^{wi,comm})$$

// calculate the predictive logits of the t-th task in Wimuse

$$\mathbf{F}_t^{st,high} = \boldsymbol{\Phi}_t^{st}(\cdot) \circ \boldsymbol{\varphi}_t^{st}(x_i)$$

// calculate the high-level feature of the t-th task in pre-trained STM.

$$\mathbf{Z}_t^{st} = \mathbf{C}_t^{st}(\cdot) \circ \boldsymbol{\Phi}_t^{st}(\cdot) \circ \boldsymbol{\varphi}_t^{st}(x_i).$$

// calculate the predictive logits of the t-th task in pre-trained STM.

Calculate $\mathbf{l}_{t,i}^{kd_1}$ (where the kd1 loss of the t-th task) by using (11).

```

        Calculate  $\mathbf{l}_{t,i}^{kd2}$  (i.e., the kd2 loss of the t-th task) by using (12).
        Calculate  $\mathbf{l}_{t,i}^{wi}$  (i.e., the final loss of the t-th task) by using (16).
    End for
     $\mathbf{L} \leftarrow \mathbf{0}$  // Initialize loss.
     $\mathbf{L} \leftarrow \sum_{t=1}^T (\omega_t \mathbf{l}_t^{wi}(\mathbf{p}_{t,n}, \mathbf{y}_{t,n}) + \lambda \mathbf{l}_{t,n}^{kd1} + \mathbf{l}_{t,n}^{kd2})$  // Update loss.
End

```

4 Experiment

In this section, we evaluate Wimuse on three public datasets under two-task and three-task sensing scenarios through using the amplitude data. As for the whole dataset, we divide 80% of them for training and 20% for testing.

CSI measured on commercial WiFi devices is well-known to contain phase offsets, including carrier frequency offset (CFO), sampling frequency offset (SFO), and symbol timing offset (STO). These phase offsets are strongly relevant to the CSI capture device, which means the phase data of various public datasets has different phase offsets and we can not use the same methods to eliminate them. In addition, we are inclined to have a more general model. Therefore, we give up the phase data of these public datasets and just use the amplitude data of them.

The pseudocode of the training scheme of Wimuse is in Algorithm 1, and the python code of Wimuse is available at <https://github.com/Zhang-xie/Wimuse>.

4.1 Datasets

ARIL dataset. ARIL dataset is proposed in [1] for the joint task of activity recognition and indoor location. Specifically, it contains the CSI samples of six gestures (i.e., up, down, left, right, circle, and cross.) in 16 locations of one room by one volunteer. In addition, the CSI samples were collected by using a pair of universal software radio peripherals (USRPs) and the total number of samples is 1440. Each sample has the shape of $1 \times 52 \times 192$, i.e. one link, 52 subcarriers, and 192 packets for one sample.

CSIDA dataset. CSIDA dataset [17] contains CSI samples of six gestures (i.e., hand left, hand right, lift, press, draw circle, and draw zigzag) in five different locations by five users. The samples are captured from laptops (i.e., one transmitter and one receiver) equipped with the Atheros CSI tool [39]. In addition, devices are set to work at monitor mode at 5 GHz to capture information of 114 subcarriers. The transmitter and receiver activate one and three antennas, respectively. Further, the sampling rate is 1000 packets per second and the gesture execution time is 1.8 seconds. There are 1500 samples with the shape $3 \times 114 \times 1800$.

Widar3.0 dataset. Widar3.0 [18] contains two sub-datasets: Dataset1 contains 12000 CSI samples collected from 16 users performing six gestures (push & pull, sweep, clap, slide, draw a circle and draw zigzag) in five different locations at three different environments, i.e., a classroom, an office, and a hall. Dataset2 holds 5,000 instances of two volunteers (one male and one female) drawing numbers 0-9 in a horizontal plane. In addition, each CSI sample in the Widar3.0 dataset is collected by six receivers and one transmitter all with three antennas. Due to the use of the 802.11n CSI tool [5], there are 30 subcarriers for each link, and send 1000 package per second. The CSI sample of one receiver has the shape of $3 \times 30 \times P$, where P represents the length of sampling from 1300 to 2200. In this work, we only adopt the samples from one receiver and Dataset1 to evaluate gesture recognition, user identification, and localization tasks.

Table 1. The architectures of the basic modules

Module	Layers	Input (No. channel \times length)	Kernel size	stride
shallow encoder	1D-Convolution	$(L * S) \times P$	7×1	2
	1D-BatchNorm	$(128 * L) \times (P/2)$	--	--
	1D-Max-pooling	$(128 * L) \times (P/2)$	3×1	2
deep encoder	1D-Convolution	$(128 * L) \times (P/4)$	3×1	1
	1D-BatchNorm	$(128 * L) \times (P/4)$	--	--
	1D-Convolution	$(128 * L) \times (P/4)$	3×1	1
	1D-BatchNorm	$(128 * L) \times (P/4)$	--	--
	1D-Convolution	$(128 * L) \times (P/4)$	3×1	2
	1D-BatchNorm	$(128 * L) \times (P/8)$	--	--
	1D-Convolution	$(128 * L) \times (P/8)$	3×1	1
	1D-BatchNorm	$(128 * L) \times (P/8)$	--	--
	1D-Convolution	$(128 * L) \times (P/8)$	3×1	2
	1D-BatchNorm	$(128 * L) \times (P/8)$	--	--
	1D-Convolution	$(128 * L) \times (P/8)$	3×1	1
	1D-BatchNorm	$(128 * L) \times (P/8)$	--	--
Classifier	1D-Convolution	$(128 * L) \times (P/8)$	3×1	1
	1D-BatchNorm	$(128 * L * 2) \times 10$	--	--
	1D-AadAvgPool	$(128 * L * 2) \times 10$	--	--
	Linear	$(128 * L * 2) \times 1$	--	--
residual adaptor	1D-Convolution	$(128 * L) \times (P/4)$	3×1	2
	1D-BatchNorm	$(128 * L) \times (P/8)$	--	--

S denotes the number of CSI subcarriers. P represents the time length of the CSI sample. L is the number of links. 1D is the abbreviation of one-dimensional. AadAvgPool is the adaptive average pooling layer.

4.2 Baselines

In this work, we compare our method Wimuse with four baselines. Note that, these baselines are constructed for CSI samples with the proposed basic modules keeping the original framework. The architecture details of the basic modules are illustrated in Table 1.

- The **STS** model for each task.
- **NMTS**: The naïve MTS model learned by minimizing the loss in (9) with the hyperparameters $\omega_t = 1$ for all tasks.
- **UMTS**: The naïve MTS model is enhanced by a principled approach [29] which weighs multiple loss functions by considering the homoscedastic uncertainty of each task to address the task unbalanced issue.
- **KDMTS**: This approach [13] addresses the unbalanced issue based on knowledge distillation. Since this method is published for joint image segmentation and depth estimation tasks, we implement this method with the abovementioned basic modules keeping the original framework.

4.3 Comparison

We compare our method to the baselines. Besides, on the ARIL dataset, we also compared it with the ARIL method [1]. We use the mean accuracy as an evaluation standard.

- **Table 2.** Performance of Various Methods on ARIL dataset (Accuracy: %)

Type	Method	Two-task Sensing		Average
		GR	IL	
STS	--	88.77	98.69	93.73
	NMTS	93.19	98.45	95.82
	ARIL	88.13	95.68	91.91
MTS	UMTS	94.15	98.80	96.48
	KDMTS	93.79	98.45	96.12
	Wimuse (ours)	95.70	99.16	97.43

GR, IL are the abbreviations of gesture recognition and indoor localization, respectively.

Results on ARIL. Firstly, we evaluate all methods on the ARIL dataset. We set the minibatch size as eight and use Adam [40] for optimizing the models. The initial learning rate is set to 0.001 and we train all methods for 500 epochs in total where we scaled the learning rate by 0.5 every 100 epochs until the 350th epoch. In Wimuse, weights of task-specific residual adaptor losses (i.e. E. (11)) and logits losses (i.e. E. (12)) are set uniformly. After the hyperparameter (λ) search, it is set 4.0 for KDMTS, and 8.0 for Wimuse. In addition, another hyperparameter (τ) to adjust the intensity of distillation is also set to 8.0 in Wimuse.

As shown in Table 2, except for the ARIL method, the MTS methods obtain better overall performance than STS, which proves that MTS models can learn more informative features than the STS model. Furthermore, ARIL obtains worse overall

performance because of its deep neural network and negligence of the abovementioned task-imbalance even task-discrepancy problem. In contrast, our method achieves significantly better performance than any other MTS method, i.e. our method achieves an accuracy of 95.70% for gesture recognition and 99.16% for indoor localization, which results from our solutions of the task-imbalance and task-discrepancy problem.

Table 3. Performance of Various Methods on Widar3.0 (Accuracy: %)

Type	Method	Two-task Sensing		Two-task Sensing		Two-task Sensing		Three-task Sensing		
		GR	IL	GR	UI	IL	UI	GR	IL	UI
STS	--	--	--	--	--	--	--	80.42	96.96	97.19
	NMTS	81.79	96.15	81.63	97.29	96.24	97.17	81.74	96.38	96.78
MTS	UMTS	80.7	96.19	82.09	97.45	95.36	97.26	81.70	96.38	96.78
	KDMTS	82.53	96.24	81.44	97.17	96.20	97.52	83.65	96.92	97.01
	Wimuse (ours)	85.27	96.84	82.46	97.59	96.46	97.91	83.79	96.73	98.05

GR, IL, and UI are the abbreviations of gesture recognition, indoor localization, and user identification.

Results on Widar3.0 dataset. Different from the experimental setup on ARIL, we performed two groups of experiments on the Widar3.0 dataset. 1) the two-task sensing including the joint gesture recognition and indoor localization task, the joint gesture recognition and user identification task, and the joint indoor localization and user identification task. 2) The three-task sensing is the joint of gesture recognition, IL, and user identification tasks. Corresponding to the four experiments, we set the hyperparameter λ and τ to the same value 2.0. Beyond this, the other experimental setups are the same as those in experiments on the ARIL dataset.

From the results shown in Table 3, we can see that it is possible to tackle multiple sensing tasks within a network and achieve performance improvement on some tasks, e.g. compared with STS on the three-task sensing experiment, the NMTS model achieves better performance on gesture recognition though it causes indoor localization and user identification to a tiny drop. Though the effectivities of using NMTS, it is also clear that the task-imbalance even task-discrepancy problem exists for the recognition accuracy of gesture recognition is lower a lot than both of that in indoor localization and user identification tasks. Then we apply existing methods for solving the task-imbalance problem. From the results of using UMTS and KDMTS, UMTS performs as well as KDMTS obtains better overall performance than NMTS. However, they perform solely better on gesture recognition but worse on indoor localization and user identification in the comparison with the STS model.

In comparison with these methods, our method obtains significant overall performance and achieves better results than other MTS models and STS, which strongly verifies the effectiveness of our proposed strategies for feature-logits distillation and compensation of the task-specific features.

Table 4. Performance of Various Methods on CSIDA (Accuracy: %)

Type	Method	Two-task Sensing		Two-task Sensing		Two-task Sensing		Three-task Sensing		
		GR	IL	GR	UI	IL	UI	GR	IL	UI
STS	--	--	--	--	--	--	--	80.26	99.64	99.82
MTS	NMTS	82.31	99.76	83.24	99.88	99.82	99.97	84.30	99.82	99.40
	UMTS	70.12	99.94	80.02	99.98	99.88	99.88	78.38	99.76	99.82
	KDMTS	81.78	99.94	83.13	99.88	99.92	99.76	82.72	99.88	99.94
	Wimuse (ours)	83.07	99.94	83.48	99.24	99.92	99.82	84.53	99.94	99.97

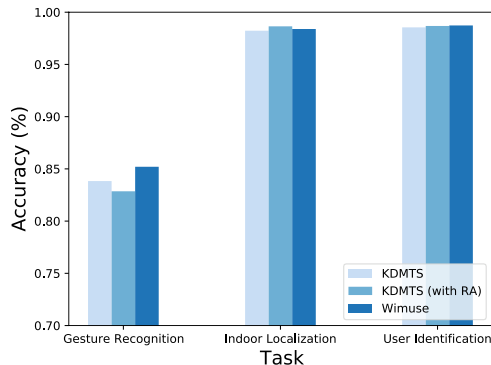
GR, IL, and UI are the abbreviations of gesture recognition, indoor localization, and user identification.

Results on CSIDA. Similar to Widar 3.0, we set the hyperparameter λ and τ to the same value for four different experiments, respectively $\lambda = 2.0$ and $\tau = 2.0$, as well.

As shown in Table 4, except for UMTS, the MTS models obtain better performance on gesture recognition tasks than the STS model and almost as excellent performance on indoor localization and user identification as the STS model. We assume that the UMTS may merely fit for applications in computer vision because its performance worse than NMTS. In addition, KDMTS performs slightly worse than NMTS, and our method remains outstanding performance among these methods.

4.4 Discussion

To better analyze the effect of the task-specific residual adaptor and the logits distillation, we conduct an ablation study on three datasets.

**Fig. 2.** The effects of the task-specific residual adaptor and the logits distillation

Analysis of task-specific residual adaptor. As mentioned in Section 3, we proposed the residual adaptor (RA), which can extract the task-specific compensation feature from the low-level features, to deal with the discrepancy issue.

From the result shown in Fig. 2, adding the task-specific RA in the KDMTS model obtains better performance on indoor localization and user identification than that it. However, it does not boost the performance of gesture recognition. As for this, we think the reason is that there is a lack of supervised information to train the RA. Since the loss of KDMTS is only related to the common feature extraction and the final predicted labels, we introduce the logits distillation to supply enough information for training.

Analysis of logits distillation. As mentioned above, we considered that the supervised information is not enough to train an excellent RA. Then we add logits distillation to sufficiently exploit the trained STS models and enrich the supervised information for Wimuse, which is proved to be extremely efficient.

As presented in Fig. 2, it is clear that Wimuse, adding the logits distillation, achieves a significantly better overall performance. As we expected, the logits distillation brought more information from the trained STS models to Wimuse for better performance.

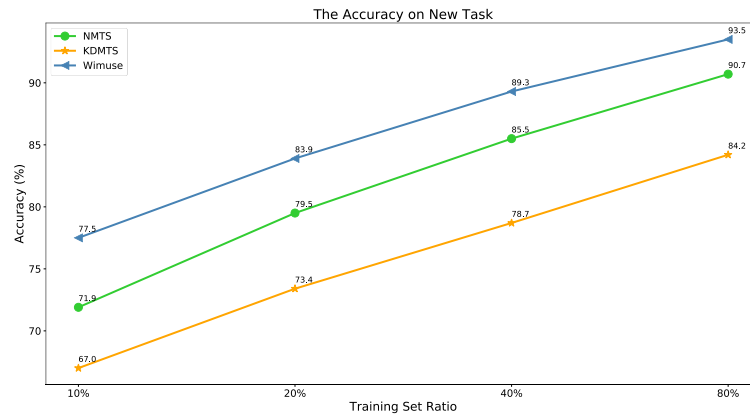


Fig. 3. The effects of the task-specific residual adaptor and the logits distillation

Analysis of task scalability. We conduct experiments on CSIDA and Widar3.0 datasets to evaluate the task scalability of Wimuse. Specifically, we construct the three-task version model by adding some modules to the pre-trained two-task version model. Then, we trained the added parts of the three-task version with the new task.

As shown in figure 3, the accuracies of NMTS, KDMTS, and Wimuse increase steadily along with the growth of the training set ratio. Further, Wimuse achieves higher accuracy than the other two models, which shows that Wimuse has better task scalability than other models. And the learned common features are more general than those in other models.

Table 5. The comparison of different methods.

Type	Method	No. Parameters	No. Multi-adds (Million)	Memory (MB)	Time (ms)
STS	For GR task	674,566	285.56	16.18	46.243
	For IL task	677,136	285.60	16.19	45.776
	ARIL	3,490,246	480.82	29.02	50.714
	NMTS	563,222	298.20	16.00	46.767
MTS	UMTS	563,222	298.20	16.00	46.811
	KDMTS	563,222	298.20	16.00	45.831
	KDMTS (with RA)	662,038	411.45	21.12	46.243
	Wimuse (ours)	662,038	411.45	21.12	46.243

‘No. parameters’ denotes the number of the trainable parameters. ‘No. Multi-adds’ represents the number of multiplexes and addition operations in labeling a new sample. ‘Memory’ and ‘Time’ are the storage memory and time needed in labeling a new sample, respectively.

Analysis of model complexity and computational cost. We also compare the model complexity, memory consumption, and runtime under the joint task of gesture recognition and indoor localization on the ARIL dataset. The input size is 52×192 with batch size as 16. As table 5 demonstrated, the MTS methods (except the ARIL method) have fewer parameters, operations, memory consumption, and runtime. It proves that MTS methods consume less, but is more efficient. In addition, compare with other MTS methods, KDMTS (with RA) and Wimuse increased the computational cost and model complexity. But it is still better than ARIL on computational cost and model complexity.

5 Conclusion

In this paper, we propose a WiFi-based multi-task sensing model (Wimuse) to perform gesture recognition, user identification, and indoor localization simultaneously. First, We reveal the imbalance and discrepancy issues in WiFi-based MTS. Then, we adopt the knowledge distillation technique and task-specific residual adaptor to address these issues. Next, we conduct comprehensive experiments on three public datasets (i.e., the ARIL dataset, the CSIDA dataset, and the Widar3.0 dataset). The evaluation suggests that Wimuse achieves state-of-the-art performance with the average accuracy of 85.20%, 98.39%, and 98.725% on the joint task of gesture recognition, indoor localization, and user identification task respectively.

Though we get satisfying results on Wimuse, there exists still two aspects for improvement, which are that we make no use of the phase data of CSI and we just achieve three tasks simultaneously. There are several fruitful directions for future investigation. i) Wimuse adopt CNN to extract features from the CSI samples. The CSI is time-series data while CNN is not suitable for sequence data. We need to adjust Wimuse to adapt the streaming data. ii) There are other more tasks that we need to exploit for the WiFi-based MTS, such as breath detection, user orientation estimation, fall detection. iii) Since the CSI can be captured from a commercial WiFi

device, we can try to deploy Wimuse into the WiFi device. And this requires a lightweight design of Wimuse to satisfy the limitations of memory, computing power in WiFi devices. iv) We can try to utilize the phase data of CSI by developing a general phase denoise method to achieve better performance.

References

- [1] F. Wang, J. Feng, Y. Zhao, X. Zhang, S. Zhang, and J. Han, "Joint Activity Recognition and Indoor Localization With WiFi Fingerprints," *IEEE Access*, vol. 7, pp. 80058–80068, 2019, doi: 10.1109/ACCESS.2019.2923743.
- [2] H. Jiang, C. Cai, X. Ma, Y. Yang, and J. Liu, "Smart home based on WiFi sensing: A survey," *IEEE Access*, vol. 6, pp. 13317–13325, 2018.
- [3] Y. Ma, G. Zhou, S. Wang, H. Zhao, and W. Jung, "SignFi: Sign Language Recognition Using WiFi," *Proc. ACM Interact. Mob. Wearable Ubiquitous Technol.*, vol. 2, no. 1, p. 23:1-23:21, Mar. 2018, doi: 10.1145/3191755.
- [4] M. Atif, S. Muralidharan, H. Ko, and B. Yoo, "Wi-ESP—A tool for CSI-based Device-Free Wi-Fi Sensing (DFWS)," *J Comput Des Eng*, doi: 10.1093/jcde/qwaa048.
- [5] D. Halperin, W. Hu, A. Sheth, and D. Wetherall, "Tool release: gathering 802.11n traces with channel state information," *SIGCOMM Comput. Commun. Rev.*, vol. 41, no. 1, p. 53, Jan. 2011, doi: 10.1145/1925861.1925870.
- [6] W. Jiang *et al.*, "Towards Environment Independent Device Free Human Activity Recognition," in *Proceedings of the 24th Annual International Conference on Mobile Computing and Networking*, New York, NY, USA, Oct. 2018, pp. 289–304. doi: 10.1145/3241539.3241548.
- [7] Z. Yang, Z. Zhou, and Y. Liu, "From RSSI to CSI: Indoor localization via channel response," *ACM Comput. Surv.*, vol. 46, no. 2, p. 25:1-25:32, Dec. 2013, doi: 10.1145/2543581.2543592.
- [8] Y. Zhang, Y. Zheng, G. Zhang, K. Qian, C. Qian, and Z. Yang, "GaitID: Robust Wi-Fi Based Gait Recognition," in *Wireless Algorithms, Systems, and Applications*, Cham, 2020, pp. 730–742. doi: 10.1007/978-3-030-59016-1_60.
- [9] D. Zhang, Y. Hu, Y. Chen, and B. Zeng, "BreathTrack: Tracking indoor human breath status via commodity WiFi," *IEEE Internet of Things Journal*, vol. 6, no. 2, pp. 3899–3911, 2019.
- [10] S. Tan, L. Zhang, Z. Wang, and J. Yang, "MultiTrack: Multi-User Tracking and Activity Recognition Using Commodity WiFi," in *Proceedings of the 2019 CHI Conference on Human Factors in Computing Systems*, New York, NY, USA, May 2019, pp. 1–12. doi: 10.1145/3290605.3300766.
- [11] R. H. Venkatnarayan, S. Mahmood, and M. Shahzad, "WiFi based Multi-User Gesture Recognition," *IEEE Transactions on Mobile Computing*, 2019.
- [12] C. Li, M. Liu, and Z. Cao, "WiHF: Enable User Identified Gesture Recognition with WiFi," 2020, pp. 586–595.
- [13] W.-H. Li and H. Bilen, "Knowledge Distillation for Multi-task Learning," in *European Conference on Computer Vision*, 2020, pp. 163–176.

- [14] K.-K. Maninis, I. Radosavovic, and I. Kokkinos, "Attentive single-tasking of multiple tasks," in *Proceedings of the IEEE/CVF Conference on Computer Vision and Pattern Recognition*, 2019, pp. 1851–1860.
- [15] G. Hinton, O. Vinyals, and J. Dean, "Distilling the Knowledge in a Neural Network," *arXiv:1503.02531 [cs, stat]*, Mar. 2015, Accessed: May 02, 2021. [Online]. Available: <http://arxiv.org/abs/1503.02531>
- [16] S.-A. Rebuffi, H. Bilen, and A. Vedaldi, "Efficient Parametrization of Multi-Domain Deep Neural Networks," 2018, pp. 8119–8127. Accessed: May 21, 2021. [Online]. Available: https://openaccess.thecvf.com/content_cvpr_2018/html/Rebuffi_Efficient_Parametrization_of_CVPR_2018_paper.html
- [17] P. Hu, C. Tang, K. Yin, and X. Zhang, "WiGR: A Practical Wi-Fi-Based Gesture Recognition System with a Lightweight Few-Shot Network," *Applied Sciences*, vol. 11, no. 8, Art. no. 8, Jan. 2021, doi: 10.3390/app11083329.
- [18] Y. Zheng *et al.*, "Zero-Effort Cross-Domain Gesture Recognition with Wi-Fi," in *Proceedings of the 17th Annual International Conference on Mobile Systems, Applications, and Services*, New York, NY, USA, Jun. 2019, pp. 313–325. doi: 10.1145/3307334.3326081.
- [19] T. Li, C. Shi, P. Li, and P. Chen, "A Novel Gesture Recognition System Based on CSI Extracted from a Smartphone with Nexmon Firmware," *Sensors*, vol. 21, no. 1, p. 222, 2021.
- [20] H. Zou, J. Yang, Y. Zhou, L. Xie, and C. J. Spanos, "Robust WiFi-Enabled Device-Free Gesture Recognition via Unsupervised Adversarial Domain Adaptation," in *2018 27th International Conference on Computer Communication and Networks (ICCCN)*, Jul. 2018, pp. 1–8. doi: 10.1109/ICCCN.2018.8487345.
- [21] J. Gjengset, J. Xiong, G. McPhillips, and K. Jamieson, "Phaser: Enabling phased array signal processing on commodity WiFi access points," in *Proceedings of the 20th annual international conference on Mobile computing and networking*, 2014, pp. 153–164.
- [22] K. Wu, J. Xiao, Y. Yi, M. Gao, and L. M. Ni, "FILA: Fine-grained indoor localization," in *2012 Proceedings IEEE INFOCOM*, Mar. 2012, pp. 2210–2218. doi: 10.1109/INFOCOM.2012.6195606.
- [23] W. Liu, H. Chen, Z. Deng, X. Zheng, X. Fu, and Q. Cheng, "LC-DNN: Local Connection Based Deep Neural Network for Indoor Localization With CSI," *IEEE Access*, vol. 8, pp. 108720–108730, 2020, doi: 10.1109/ACCESS.2020.3000927.
- [24] Y. Zhang, W. Wang, C. Xu, J. Qin, S. Yu, and Y. Zhang, "SICD: Novel Single-Access-Point Indoor Localization Based on CSI-MIMO with Dimensionality Reduction," *Sensors*, vol. 21, no. 4, Art. no. 4, Jan. 2021, doi: 10.3390/s21041325.
- [25] J. Jung, H.-C. Moon, J. Kim, D. Kim, and K.-A. Toh, "Wi-Fi Based User Identification Using In-Air Handwritten Signature," *IEEE Access*, vol. 9, pp. 53548–53565, 2021, doi: 10.1109/ACCESS.2021.3071228.
- [26] Z. Zhang, P. Luo, C. C. Loy, and X. Tang, "Facial Landmark Detection by Deep Multi-task Learning," in *Computer Vision – ECCV 2014*, Cham, 2014, pp. 94–108. doi: 10.1007/978-3-319-10599-4_7.
- [27] A. Wang, A. Singh, J. Michael, F. Hill, O. Levy, and S. R. Bowman, "GLUE: A Multi-Task Benchmark and Analysis Platform for Natural Language Understanding,"

- arXiv:1804.07461 [cs]*, Feb. 2019, Accessed: May 28, 2021. [Online]. Available: <http://arxiv.org/abs/1804.07461>
- [28] L. Deng, G. Hinton, and B. Kingsbury, "New types of deep neural network learning for speech recognition and related applications: an overview," in *2013 IEEE International Conference on Acoustics, Speech and Signal Processing*, May 2013, pp. 8599–8603. doi: 10.1109/ICASSP.2013.6639344.
- [29] A. Kendall, Y. Gal, and R. Cipolla, "Multi-task learning using uncertainty to weigh losses for scene geometry and semantics," in *Proceedings of the IEEE conference on computer vision and pattern recognition*, 2018, pp. 7482–7491.
- [30] M. Guo, A. Haque, D.-A. Huang, S. Yeung, and L. Fei-Fei, "Dynamic Task Prioritization for Multitask Learning," 2018, pp. 270–287. Accessed: May 28, 2021. [Online]. Available: https://openaccess.thecvf.com/content_ECCV_2018/html/Michelle_Guo_Focus_on_the_ECCV_2018_paper.html
- [31] O. Sener and V. Koltun, "Multi-Task Learning as Multi-Objective Optimization," *arXiv:1810.04650 [cs, stat]*, Jan. 2019, Accessed: May 28, 2021. [Online]. Available: <http://arxiv.org/abs/1810.04650>
- [32] S. Sun, Y. Cheng, Z. Gan, and J. Liu, "Patient knowledge distillation for bert model compression," *arXiv preprint arXiv:1908.09355*, 2019.
- [33] J. Yim, D. Joo, J. Bae, and J. Kim, "A gift from knowledge distillation: Fast optimization, network minimization and transfer learning," in *Proceedings of the IEEE Conference on Computer Vision and Pattern Recognition*, 2017, pp. 4133–4141.
- [34] M. Orbes-Arteainst *et al.*, "Knowledge distillation for semi-supervised domain adaptation," in *OR 2.0 Context-Aware Operating Theaters and Machine Learning in Clinical Neuroimaging*, Springer, 2019, pp. 68–76.
- [35] S. Kumar, B. Banerjee, and S. Chaudhuri, "Online sensor hallucination via knowledge distillation for multimodal image classification," *arXiv preprint arXiv:1908.10559*, 2019.
- [36] D. Xu, W. Ouyang, X. Wang, and N. Sebe, "Pad-net: Multi-tasks guided prediction-and-distillation network for simultaneous depth estimation and scene parsing," in *Proceedings of the IEEE Conference on Computer Vision and Pattern Recognition*, 2018, pp. 675–684.
- [37] S. Chelaramani, M. Gupta, V. Agarwal, P. Gupta, and R. Habash, "Multi-Task Knowledge Distillation for Eye Disease Prediction," 2021, pp. 3983–3993. Accessed: May 28, 2021. [Online]. Available: https://openaccess.thecvf.com/content/WACV2021/html/Chelaramani_Multi-Task_Knowledge_Distillation_for_Eye_Disease_Prediction_WACV_2021_paper.html
- [38] K. He, X. Zhang, S. Ren, and J. Sun, "Deep Residual Learning for Image Recognition," 2016, pp. 770–778. Accessed: Oct. 23, 2020. [Online]. Available: https://openaccess.thecvf.com/content_cvpr_2016/html/He_Deep_Residual_Learning_CVPR_2016_paper.html
- [39] Y. Xie, Z. Li, and M. Li, "Precise Power Delay Profiling with Commodity Wi-Fi," *IEEE Transactions on Mobile Computing*, vol. 18, no. 6, pp. 1342–1355, Jun. 2019, doi: 10.1109/TMC.2018.2860991.
- [40] D. P. Kingma and J. Ba, "Adam: A method for stochastic optimization," *arXiv preprint arXiv:1412.6980*, 2014.